To appear in J. Mech. Phys. Solids

DYNAMIC FLOW AND FAILURE OF CONFINED POLYMETHYLMETHACRYLATE

D. Rittel* and A. Brill

Faculty of Mechanical Engineering, Technion, 32000 Haifa, Israel

ABSTRACT

The static and dynamic mechanical behavior of confined commercial polymethylmethacrylate (PMMA) is investigated. Cylindrical specimens are confined by means of a tightly fit metal sleeve and subjected to compression tests. The rate and pressure sensitivity of PMMA are characterized over a range of strain rates of $\dot{\varepsilon} = 10^{-3} - 10^{4}\,\mathrm{s}^{-1}$. In the quasi static regime, the material is quite ductile, exhibiting noticeable barreling. The dynamic failure mode consists of axial splitting and fragmentation at the lower strain rates $\left(\dot{\varepsilon} < 2000\,\mathrm{s}^{-1}\right)$ and confining pressures. But, at the higher strain rates and confining pressures, the failure mode changes to adiabatic shear formation of a conical plug. This failure mode transition, identified by SEM fractographic analysis, can be explained by the fact that the confinement delays the operation of damage micromechanisms, as evidenced from the post-peak slope. The response of this polymer is described using a fitted rate-dependent Drucker-Prager pressure-sensitive model, according to: $\tau_{\mathrm{flow}} = 66.78\dot{\gamma}^{0.06933} + 0.223\mathrm{p}$, for $10^{-3} \le \dot{\gamma} \le 10^{4}\,\mathrm{s}^{-1}$. This work shows that confining PMMA turns this brittle material into a ductile one, exactly like for other brittle materials such as ceramics. The present results thus fit into a general description of the pressure induced brittle-ductile transition, including rate sensitivity effects for this material.

KEYWORDS: PMMA, confinement, pressure sensitivity, high strain rate, adiabatic shear

(*) *Corresponding author*: merittel@technion.ac.il

INTRODUCTION

The dynamic mechanical and failure behavior of amorphous polymers has caused renewed interest, as these materials are likely to be used in structural applications involving high rate impacts. Recently published results revealed an intriguing capability of commercial polymethylmethacrylate (PMMA) panels to sustain and deflect ballistic impacts under certain conditions (Rosenberg, et al., 2005). More generally, polymers are considered as potential components of armor systems, thus calling for a fundamental evaluation of their dynamic mechanical behavior.

The mechanical properties of many polymers have been extensively studied and modeled at low strain-rates, as seen in text books on viscoelasticity (Christensen, 1982), and on their general mechanical behavior (Ward, 1983). As the strain rate increases, fewer studies are available, as in the case of fatigue (both low and high cycle). Here an additional component of the problem is the nature and extent of thermo-mechanical coupling effects in which the mechanical energy transforms readily at low frequencies into thermal energy. This causes self-heating of the material (Constable, et al., 1970; Rittel, 2000b). When the strain rate becomes higher, as in the case of impact, the thermomechanical problem becomes dominant, since very high (homologous) temperatures are likely to develop (Rittel, 1999). Dynamic experiments on glassy polymers are relatively scarce (Arruda, et al., 1995; Li and Lambros, 2001; Rittel, 2000a; Trojanowski, et al., 1997), and they essentially concentrate on the more ductile polymers. The dynamic behavior of the so-called *brittle polymers* has attracted less attention, except for the fact that the material is often considered as a model material such as Homalite (Knauss and Ravi-Chandar, 1985). Commercial polymethylmethacrylate (PMMA), which can be considered as a brittle material (at high strain rates), was characterized by Kolsky (1949) from a constitutive point of view, and later by Rittel (2000c), from both a constitutive and a fracture point of view. It is basically agreed that PMMA is highly rate sensitive, and while it can undergo large deformations at low strain rates, this material tends to fragment readily at high strain rates. So far, PMMA has caused only limited research interest due to its propensity to fragmentation at high strain rates, which severely limits its applications.

In what appears as a totally different context, the general issue of brittle material failure has attracted recent attention, at least for rocks and geomaterials, as can be found in recent papers by Renshaw and Schulson (2001) and by Ramsey and Chester (2004). Here, the materials were confined during testing, and it was shown that the confinement acts in delaying failure

micromechanisms that would usually operate (nucleation and coalescence) in the brittle material to cause its final failure. Here one should of course mention the pioneering work of Bridgman (1945) on the role of the hydrostatic pressure on the failure of metals. More recently, Chen and Ravichandran (1997) were among the first to investigate dynamic confinement effects on a brittle ceramic. These authors revealed and modeled a failure mode transition to a ductile shear failure at high levels of confinement.

At this stage, an interesting observation, due to Winter (1975), should be mentioned. This author performed punching experiments with a cylindrical rod pressed onto titanium alloy and PMMA plates. A striking similarity was reported in terms of failure mode by localized shear (cones) that formed in the plates of either investigated material. Later, Satapathy and Bless (2000) performed dynamic punching experiments on PMMA and showed that confinement of this material may postpone cracking at the benefit of a ductile shear failure mechanism, bearing a definite similarity with Winter's (1975) results.

One can now link the various parts of this introductory section by invoking and reviewing hydrostatic pressure effects. First, the punching process produces a high hydrostatic pressure (analogous to confinement), and thus leads to the ductile failure of a nominally brittle polymeric material. For another brittle material (ceramic), confinement is also found to induce a ductile-like failure, for dynamic loading. So, as a general observation, it is now well established that the confinement of brittle materials may cause their dynamic failure to occur by a ductile mechanism.

However, the effects of external confinement on commercial PMMA have not yet been investigated, for both its dynamic constitutive response and failure mechanism(s). This is precisely the goal of the present investigation.

The paper is therefore organized as follows: the first section describes the experimental procedure, namely how to apply and measure a hydrostatic confinement to a cylindrical specimen using a ductile metal sleeve. The next section shows typical quasi-static and dynamic stress-strain curves that are used to illustrate the strain-rate and pressure sensitivity of PMMA. An excellent agreement with previous work on un-confined PMMA is shown. The first issue to be addressed is that of the pressure-sensitivity of this material at various strain rates. It is shown here that PMMA seems to retain its pressure sensitivity at high strain rates. The nature of the failure process (in the post-peak regime) is also characterized. When higher strain rates and pressures are applied, a dramatic change of failure mode, from radial fragmentation to adiabatic shear banding, is noted for a well defined regime of pressures and strain rates. The third section presents a detailed fractographic study of the various observed

failure modes. The fourth section discusses and summarizes the main results of this work, introducing a simple constitutive relationship that accounts for the rate and pressure dependence of the mechanical properties. The discussion also addresses the observed failure mode transition in the more general context of pressure dependent behavior, thus establishing a link with previous observations. This section is followed by concluding remarks.

EXPERIMENTAL

Specimens and confinement

Cylindrical specimens, 6 mm diameter - 6 mm high, were machined from 12.7 mm diameter cylindrical bars of commercial PMMA. All the specimens of this study were machined from the same bar. The confining pressure was applied by means of a metallic sleeve, similar to the technique used by Hanina et al. (2007), as shown in Figure 1. The main idea is that the sleeve is designed to yield at the *early* stages of the test, and being made of a low strain-hardening material, it applies a relatively *constant pressure* to the specimen.

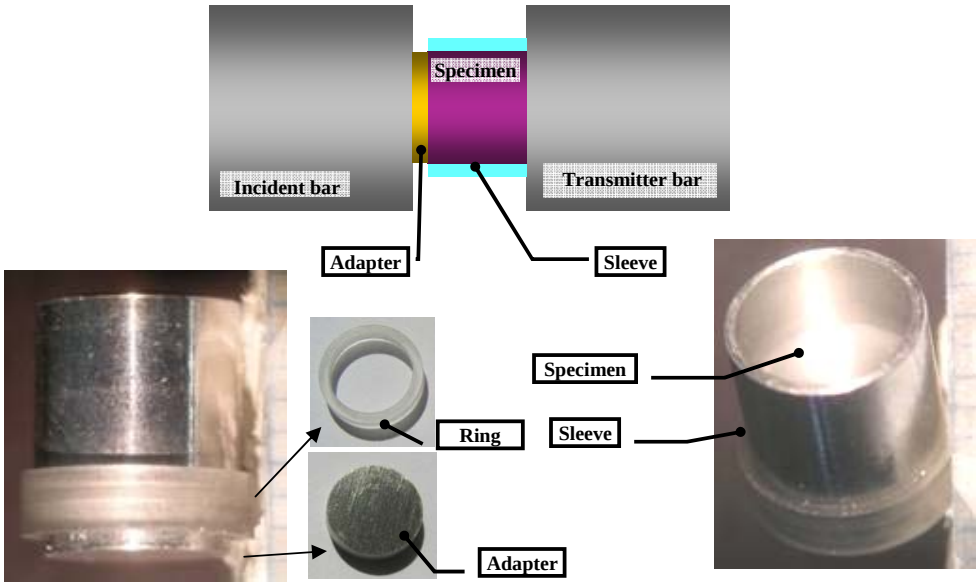

Figure 1: Experimental technique to confine and load a compression specimen.

Figure 2 shows schematically the confining effect of the metallic sleeve on the cylindrical specimen. For metals, the flow stress is only affected by the strain-rate irrespective of q. Polymers, by contrast, are both pressure and strain-rate sensitive materials. Considering only pressure-sensitivity at this stage, the measured stress component of a confined compression

test is $\sigma_{11}^{meas} = \sigma_{11}(q) + q$, where q is the confining pressure. For a pressure-insensitive material, $\sigma_{11}(q) \equiv \sigma_{11}^{u}$, where the superscript u stands for unconfined. Therefore, q could be directly determined by subtracting the unconfined from the confined curve, as shown by Hanina et al. (2007) and by Rittel et al. (2007). Here, pressure sensitivity requires that q be calculated separately, and be subtracted from the measured axial stress in order to determine $\sigma_{11}(q)$. Throughout this work, $\sigma_{11}(q)$ consistently stands for the measured stress σ_{11}^{meas} from which the confining pressure q has been subtracted. The detailed procedure used to assess q is explained in the Appendix section.

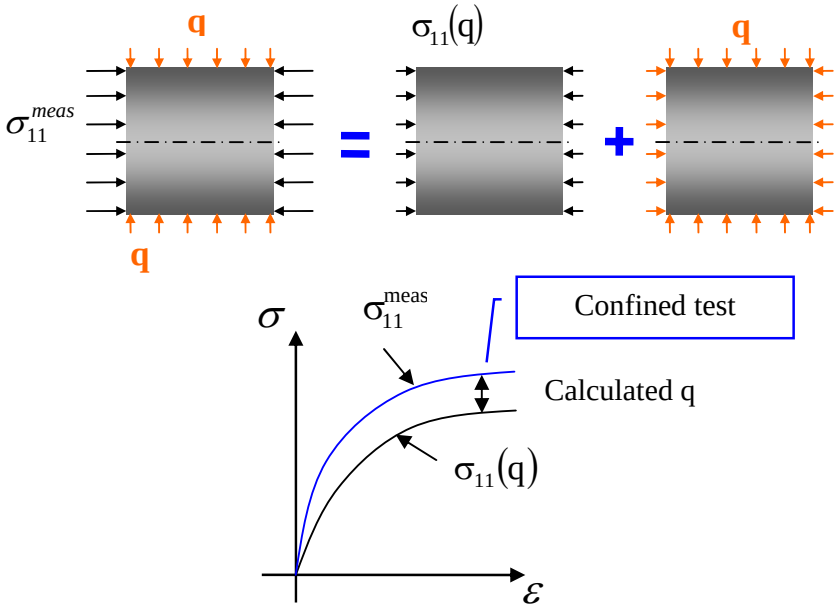

Figure 2: Stress state of a confined specimen. Note that q is calculated separately, to determine the flow stress at a given level of confinement.

The specimen was encased in accurately machined sleeves made of 6061-T651 aluminum alloy (Figure 1), with a wall thickness, $t = 0.3, 0.5, \text{and } 0.7 \pm 0.005$ mm respectively. The internal diameter of the sleeves was accurately machined to tightly match that of the specimen, which was inserted by applying a small hand pressure to it. Friction between the specimen and the sleeve is deemed to be negligible in these experiments, and will therefore not be considered. The sleeve material and dimensions were optimized so that the confining pressure q was reasonably constant, starting from low strains (typically $\varepsilon \approx 0.05$), as could be seen in numerical simulations (Appendix). The specimen was loaded through a 2 mm thick adapter made of 6061-T651 aluminum alloy (Figure 1). The adapter diameter was carefully

adjusted to that of the specimen, to avoid loading of the sleeve. The adapter was aligned with the specimen by means of a polymeric centering ring (Figure 1).

Mechanical testing

Un-confined and confined specimens were tested in uniaxial compression. Quasi-static tests were tested at room temperature under displacement-control on a servo-hydraulic testing machine (MTS 810). Compression tests were carried out with an extensometer attached to the specimen, so that machine compliance effects were avoided.

Dynamic tests were conducted on a 12.7mm diameter - 250 Maraging steel apparatus (split Hopkinson pressure bar (Kolsky, 1949), with the adapter always facing the incident bar. Special care was paid to optimize the dimensions of the adapter so that it did not distort the recorded stress waves. The transmitter bar of the setup is significantly shorter than the incident bar to ensure that the specimen is not repeatedly loaded by the stress waves (Chen and Ravichandran, 1996). Following every impact test, it was checked that the aluminum adapter did not suffer any permanent strain or damage. The uniaxial stress-strain curves were determined in a standard way after checking for dynamic equilibrium of the specimen.

Since PMMA is rate-sensitive, quasi-static and dynamic tests were conducted in pairs for each wall thickness of the sleeve.

RESULTS

Stress-strain curves

Quasi-static testing

Figure 3(a) shows typical true stress-strain curves (determined based on material incompressibility as a first approximation), for various levels of confinement. The curves are identical in shape, and they are shifted on the stress axis by the (calculated) value of the confining pressure q. The material exhibits a high level of ductility, as witnessed by the large compressive strain achieved. One should note that the specimens did not fail, but tended to barrel at larger strains. Figure 3(b) illustrates the similarity of the flow curves, once the confining pressure has been subtracted, emphasizing the pressure sensitivity of the material.

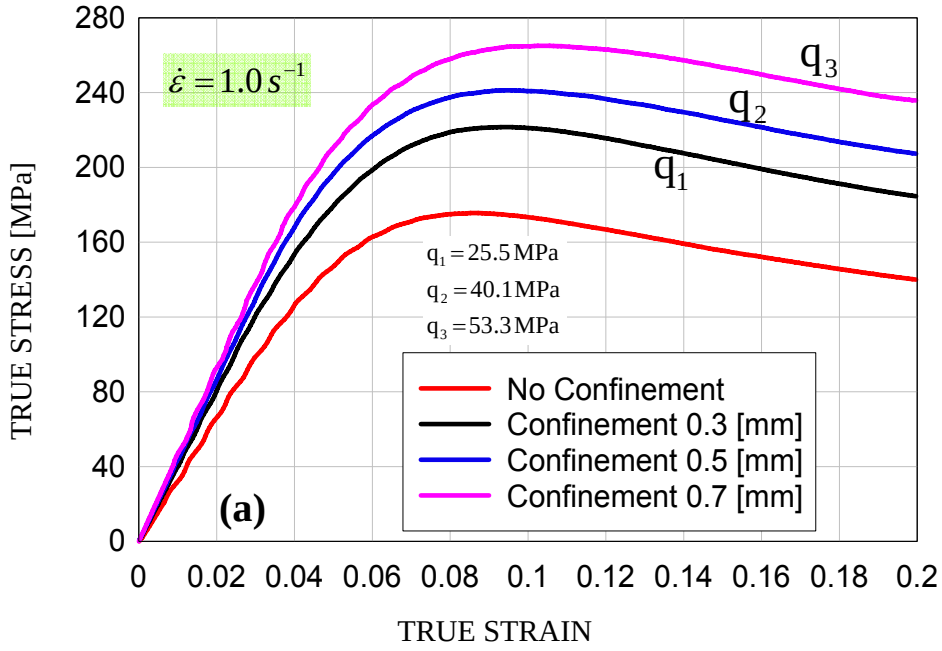

Figure 3a: (a) Typical quasi-static tests results. The label *q* indicates confinement. The stress is σ_{11}^{meas}.

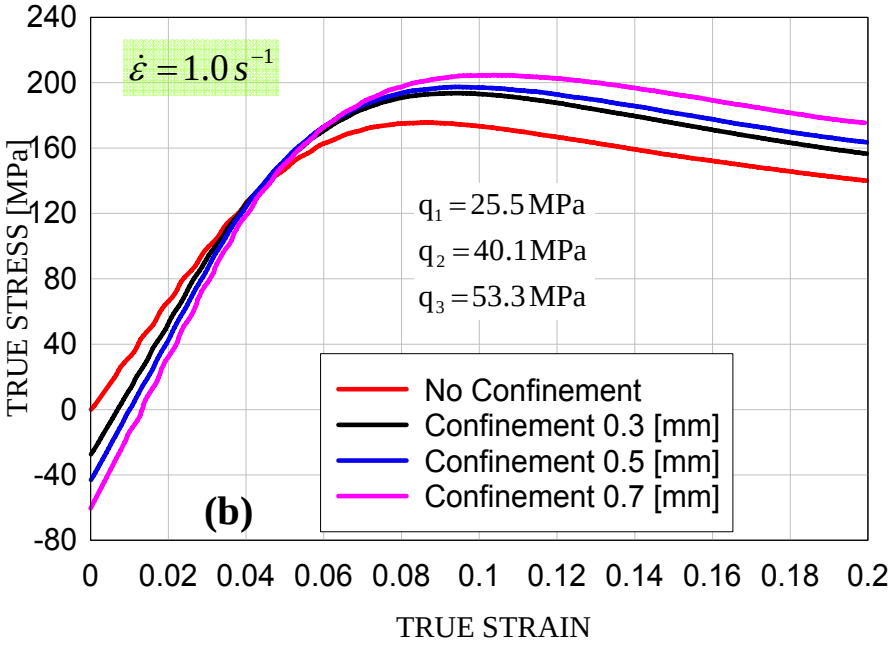

Figure 3b: Identical to (a), after subtraction of calculated *q* so that the stress is now $\sigma_{11}(q)$. Note the similarity of the curves.

Dynamic testing

Figure 4 shows typical stress strain curves for the dynamic regime. As the material is strain-rate sensitive, Figure 4 compares various confinement levels at an identical strain rate of $\dot{\varepsilon} \approx 2000\, s^{-1}$. As expected, the flow stress of the material increases with the confining pressure. It is also interesting to compare the various post-peak slopes as a function of the applied *q*. Two typical domains with characteristic slopes follow the peak load on these plots. These domains are dictated by the failure mechanisms that cause strain softening. The first, immediately following the plateau stress, has a milder slope and it probably corresponds to damage nucleation and growth. By contrast, the second has a much steeper slope, and it corresponds to final failure. While the second slope (final failure) appears to be rather constant for each case, it clearly appears that, as *q* increases, the first slope becomes milder, indicating an increasingly controlled type of failure. Overall, Figure 4 clearly shows that the material has a higher ductility to failure, when *q* is increased, ductility being defined here as the strain at which the post peak slope changes markedly indicating the onset of final failure. It is also important to note that *in all these cases*, the specimens fail by radial cracking that causes fragmentation into numerous small fragments (Rittel, 2000c). The unconfined specimen produces many more small fragments than the confined specimens.

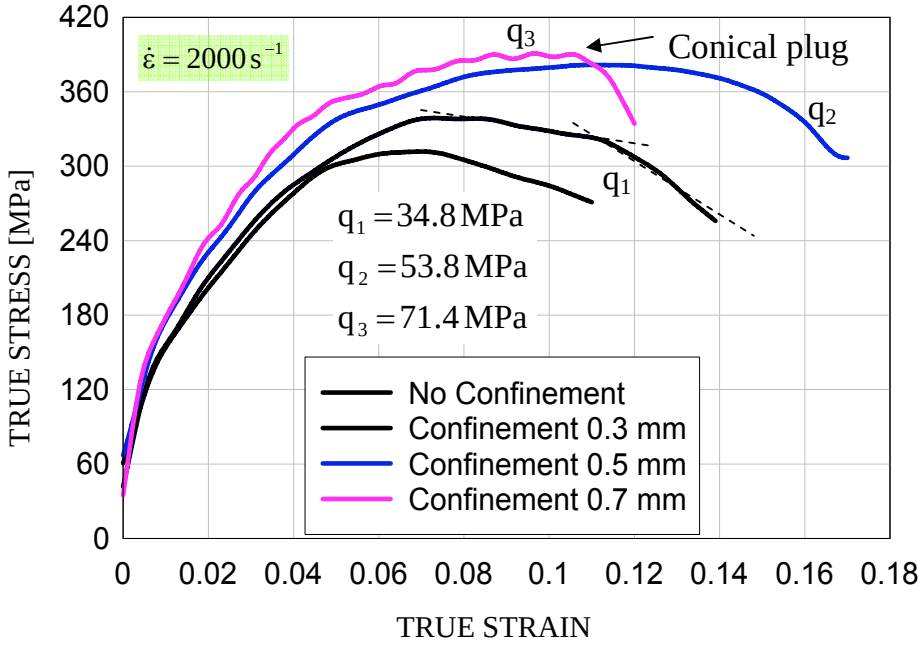

Figure 4: Typical dynamic test results where the stress is σ_{11}^{meas}.Note that when q_3 reaches 71.4 MPa, at $\dot{\varepsilon} = 2000\,s^{-1}$, failure occurs by the formation of a conical

plug rather than by radial fragmentation. The dashed lines on the q_1 curve outline the 2 slopes that characterize the failure process. The first slope gets increasingly milder at higher confining pressures.

However, this trend is brutally interrupted when q is again increased to $q=q_3$ level in Figure 4. Here, instead of showing additional ductility, the specimen fails at a much smaller strain ($\varepsilon \approx 0.115$), and a truncated conical plug is formed on the impacted side. At this stage, one should remember that the confining pressure has been increased at a fixed strain rate, and the failure mode is observed to change dramatically to what seems to be adiabatic shear banding, as discussed in the sequel.

The strain rate sensitivity of commercial PMMA is illustrated in Figure 5. The measured peak stress $\left(\sigma_{11}^{meas}\right)$ is plotted as a function of the strain rate together with the results of other authors for unconfined tests. Figure 5 shows an excellent agreement with the previously published results, indicating a qualitatively similar rate-dependence for the confined tests.

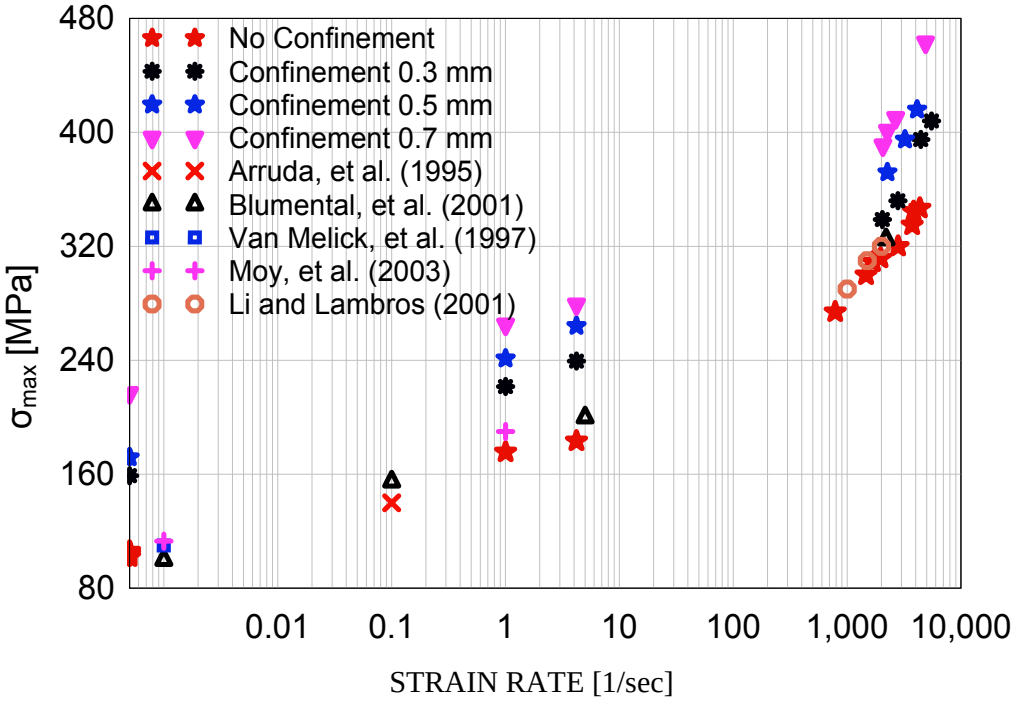

Figure 5: A summary of the peak stress $\left(\sigma_{11}^{meas}\right)$ vs. strain rate, including previously reported results (Arruda, et al., 1995; Blumental, et al., 2001; Li and Lambros, 2001; Moy, et al., 2003; Van-Melick, et al., 1997).

Figure 6 re-plots part of data shown in Figure 5, with the addition of circles to outline those specimens for which a conical plug was clearly observed. While conical plug formation

obviously requires a confining pressure, Fig. 6 indicates qualitatively that plug formation at increasing levels of confinement lower the strain rates at which plugging occurs.

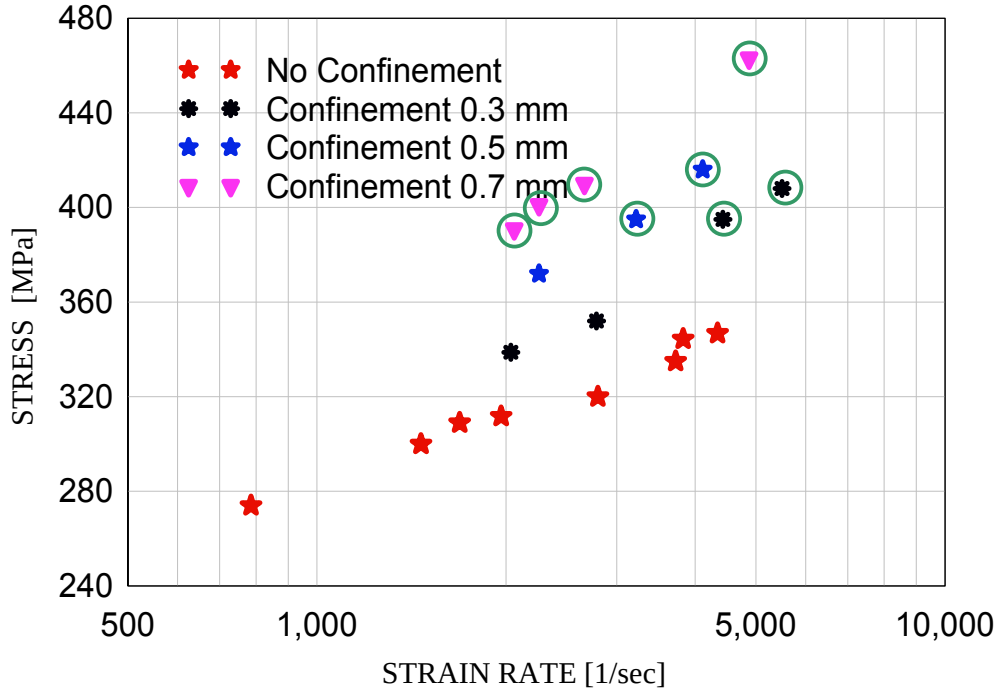

Figure 6: Data points shown in Figure 6, with circles indicating conical plug formation. Note that at the lower strain rates, plug formation requires a higher confining pressure. The unconfined specimens all failed by shattering.

Fractographic analysis

Figure 7 shows the fracture mechanism(s) operating during radial cracking at the lower strain rates/confinement levels. The typical morphologies correspond to featureless (mirror) or rough landscape (hackles) according to the local crack velocity. In any case, these features are characteristic of "brittle" failure of glassy polymers (Rittel and Maigre, 1996) and other traditional brittle materials such as glasses. For this case, the usual failure criterion is that of a maximum normal stress that enforces a crack-opening mode.

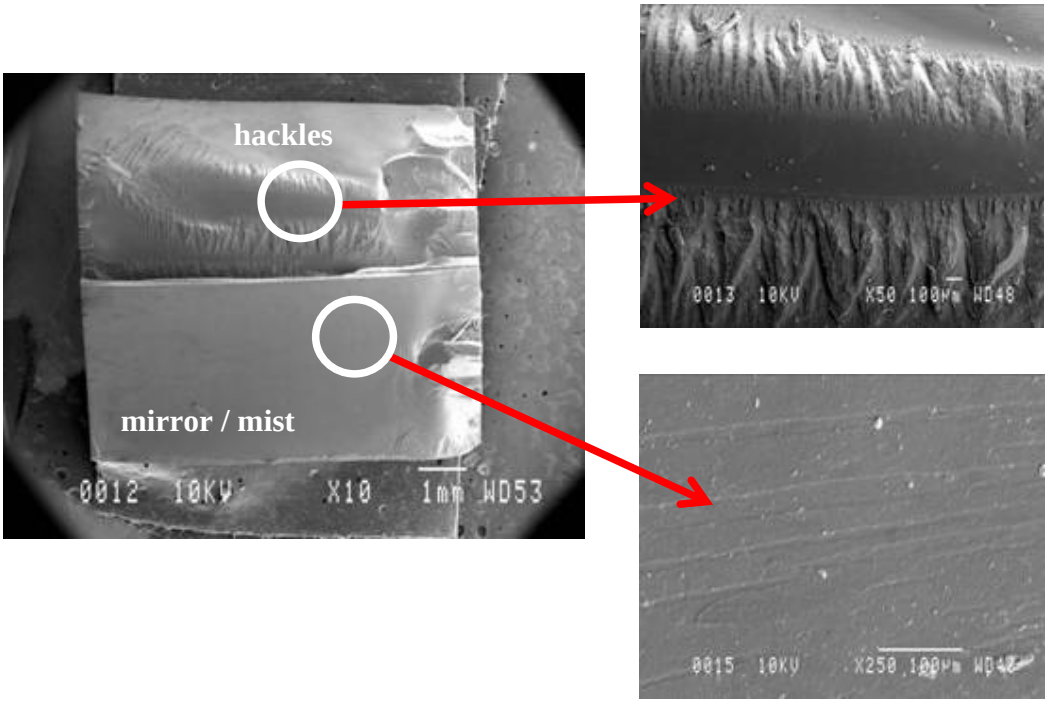

Figure 7: Fracture surfaces of radial fragments. Note the mirror (mist) and hackles, indicating a "brittle" type of failure.

Figure 8 shows the conical plug that is typically observed at higher strain rates and/or confinement levels. The plug is a truncated cone with its large base being directly impacted, its smaller base being formed inside the specimen. The small base is basically featureless, corresponding again to a brittle tensile type of failure. By contrasts, the cone's envelope is essentially comprised of elongated dimples, which at higher magnification, show clear signs of material softening and/or melting. The cone envelope can be identified without ambiguity as characteristic of a ductile shear failure mechanism. The signs of thermal softening and elongated dimples, all point to the operation of adiabatic shear failure, or adiabatic shear banding (Tresca, 1879). Additional insight is gained by examining a polished cross section, taken perpendicular to the fracture plane of the plug, as shown in Figure 9. This figure discloses a damaged surface layer of approximately 10µm thick (half-band thickness). The band contains numerous microcracks or voids, and obvious signs of plastic flow. Such signs of damage are not observed outside the shear-band, and they confirm the operation of a highly localized failure mode. To conclude this section, the conical plug is undeniably formed by adiabatic shear banding.

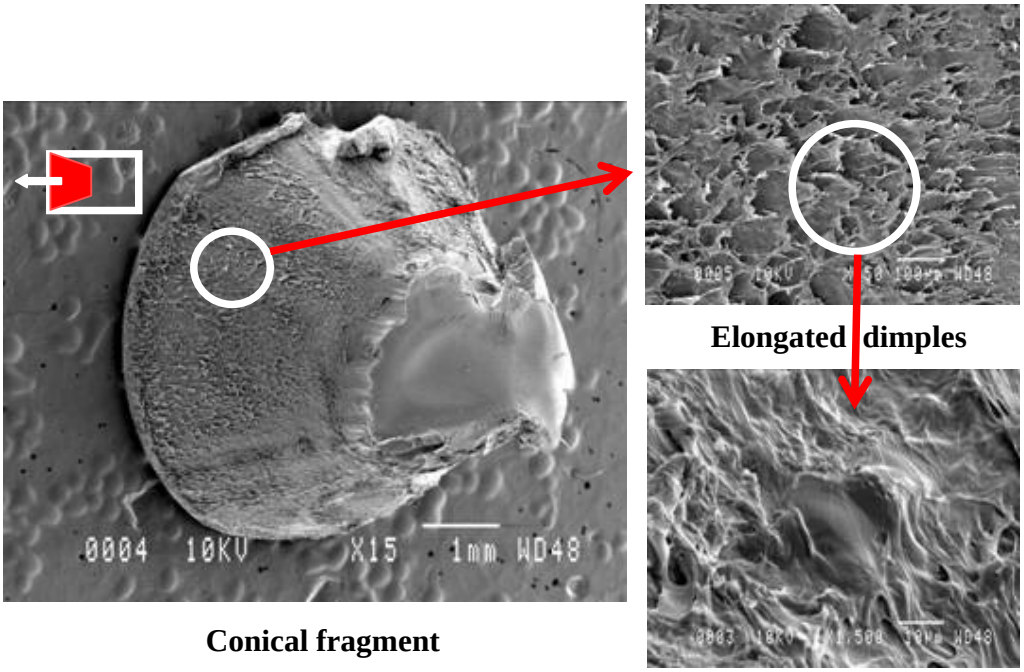

Figure 8: Typical fracture mechanisms for the conical plugs – adiabatic shear cones.

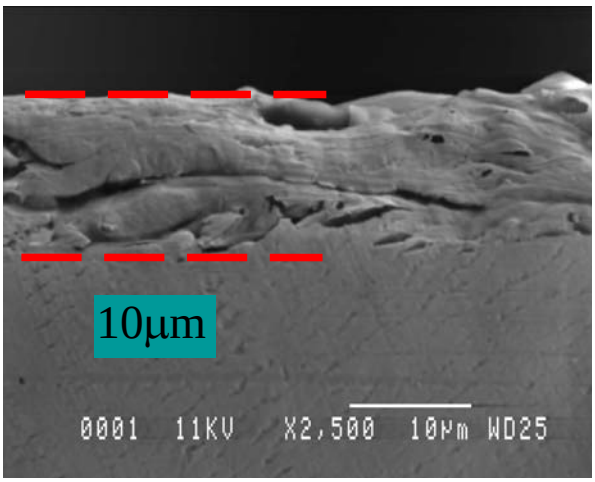

Figure 9: Typical microstructure of the adiabatic shear band (half-width). Note the multiple microcracks, as well as signs of extensive flow (layering) and damage.

DISCUSSION

This work concerns the dynamic mechanical and failure behavior of nominally brittle PMMA, which is tested under various levels of confinement. As a preliminary remark, one should note that all the results point to the fact that the material is only brittle at high strain-rates, whereas it displays a significant ductility in the quasi-static regime. It is also observed, in perfect accord with previous reports, that PMMA is a highly strain-rate sensitive material.

Specific points will now be discussed, that appear to be of prime interest, namely the pressure sensitivity of PMMA at various strain rates, and the occurrence of adiabatic shear banding as a manifestation of a pressure induced brittle-ductile failure mode transition.

Pressure sensitivity of commercial PMMA in the quasi-static and dynamic regimes

Table 1 shows various mechanical results of this study, for several specimens grouped according to the range of strain rates. Three groups are arbitrarily defined, namely (1) the very slow quasi-static regime, $\dot{\varepsilon} \approx 10^{-4}\,\mathrm{s}^{-1}$, (2) the quasi-static regime, $1 \le \dot{\varepsilon} \le 5\,\mathrm{s}^{-1}$, and (3) the dynamic regime where $10^{2} \le \dot{\varepsilon} \le 10^{4}\,\mathrm{s}^{-1}$. A representative flow stress of $\sigma_{\mathrm{flow}} = \sigma_{11}(\mathrm{q})\mathrm{at}\,\varepsilon = 0.06$ is selected to minimize thermal effects.

Group	**Strain Rate [1/s]**	**t [mm]**	**q [MPa]**	$\sigma_{\mathrm{flow}}(\varepsilon = 0.06)$ **[MPa]**		**Group**	**Strain Rate [1/s]**	**t [mm]**	**q [MPa]**	$\sigma_{\mathrm{flow}}(\varepsilon = 0.06)$ **[MPa]**
1	0.0005	0	0	100.3		3	1687	0	0	301.6
1	0.0005	0.3	25.5	123.1		3	1964	0	0	309.7
1	0.0005	0.5	40.1	116.7		3	2409	0	0	310.8
1	0.0005	0.7	53.3	130.7		3	2800	0	0	316.0
						3	2035	0.3	34.1	291.9
2	1	0	0	162.8		3	2786	0.3	34.1	308.5
2	4.2	0	0	163.5		3	2060	0.5	53.8	295.7
2	1	0.3	25.5	173.0		3	2257	0.5	53.8	300.9
2	4.2	0.3	25.5	187.2		3	2309	0.5	53.8	307.6
2	1	0.5	40.1	176.9		3	2060	0.7	71.4	292.8
2	4.2	0.5	40.1	196.6		3	2257	0.7	71.4	311.2
2	1	0.7	53.3	180.0		3	2666	0.7	71.4	317.2
2	4.2	0.7	53.3	183.4		3	3828	0	0	344.3
						3	4428	0.3	34.1	353.9
3	785	0	0	273.8		3	5500	0.3	34.1	373.9
3	964	0	0	287.5		3	3221	0.5	53.8	336.4
3	1137	0	0	286.0		3	4111	0.5	53.8	362.2
3	1428	0	0	287.1		3	4873	0.7	71.4	364.1
3	1464	0	0	290.3						

Table 1: Mechanical results. The specimens have been grouped into 3 arbitrary groups according to the strain rate. The sleeve's thickness, *t*, is given along with the calculated corresponding confining pressure, *q* and the flow stress $\sigma_{\mathrm{flow}} = \sigma_{11}(\mathrm{q})\mathrm{at}\ \varepsilon = 0.06.$

The results can be fitted according to the Drucker-Prager pressure sensitive criterion, written as:

$$\tau_{flow} = \alpha p + \tau_0 \qquad (1)$$

Where, $\tau_{flow} = \frac{1}{2}\sigma_{flow}(\varepsilon = 0.06)$, α is the pressure sensitivity and $\gamma=2\varepsilon$. The hydrostatic pressure, $p = \frac{(\sigma_{flow} + 2q)}{3}$ (see Appendix). The fitted parameters are listed in Table 2, and the results are plotted in Figure 10.

Group	**Shear strain rate** [1/s]	**α**	**τ_0** [MPa]
1	0.001	0.2230	43.47
2	2.0-8.4	0.1892	72.12
3	3374-11000	0.2436	124.2

Table 2: Drucker-Prager constants for PMMA at various strain rates.

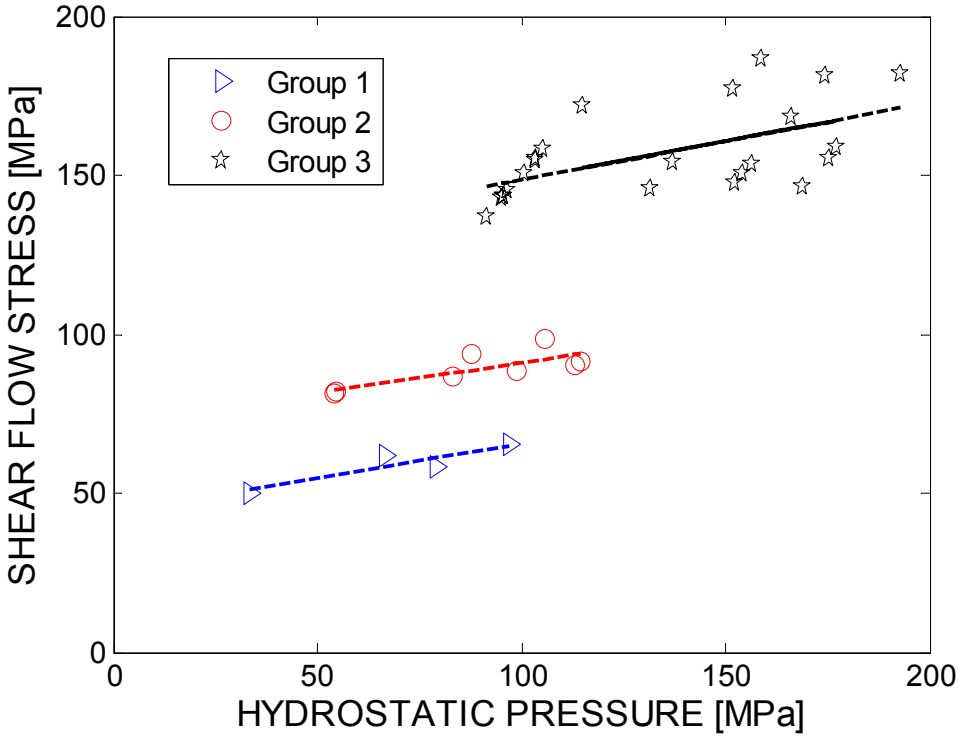

Figure 10: Shear flow stress vs. hydrostatic pressure, for the 3 groups of strain rates. The dashed lines correspond to the parameters listed in Table 2.

The first observation is that the low strain-rate values of the Drucker-Prager's parameters (α=0.223 and τ_0=43.47 MPa) are in excellent agreement with those reported by Quinson et al. (1997), of α=0.23 and τ_0=45 MPa, respectively. The measured value of the pressure sensitivity coefficient (α=0.223) corresponds to an angle of 12.57°. Bardia and Narasimhan (2006) formulate their criterion in terms of normal stresses, and report an average angle of 20.4° whose half value is very close to the parameter reported in this work. It should be noted that three very different experimental methods yield very similar results for the pressure sensitivity of PMMA, adding reliability to the reported values.

It also appears that increasing strain rates cause a slight decrease in the pressure-sensitivity index, and an increase in the reference shear stress. While the latter result is quite expected, the first issue has not really been investigated or clearly reported in the literature. One must keep in mind that 3 groups of strain rates were *arbitrarily* defined in order to calculate the pressure sensitivity parameters. Thus, one cannot conclude that the experimental results contained in Table for groups 2 and 3 are sufficient to indicate a statistically significant trend of a decreasing α with the strain rate. However, this point is quite interesting and it should obviously be further investigated by producing a large series of experimental points at carefully controlled strain rates. We will therefore assume here a conservative value of α=0.223. The dependence of the reference shear stress on the shear strain rate can be (fitted) described by $\tau_0 = 66.78\dot{\gamma}^{0.06933}\,[\mathrm{MPa}]$, assuming *representative* shear strain rates of $\dot{\gamma} = 0.001,\ 5,\ \text{and}\ 7000\,\mathrm{s}^{-1}$ for each group, respectively. The shear flow stress, calculated at γ=0.12, can now be expressed as:

$$\tau_{\text{flow}} = 66.78\dot{\gamma}^{0.06933} + 0.223\,\mathrm{p} \qquad (2)\,.$$

The pressure and strain-rate dependence of the shear flow stress are shown in Figure 11, for each set of experimental points, according to the sleeves thickness (*t* in Table 2), and their fitted counterparts (eqn. (2)). This figure shows that the experimental results are quite well approximated by the empirical equation (2), keeping in mind the simplifying assumptions made to derive this fitting, namely the 3 selected representative strain rates.

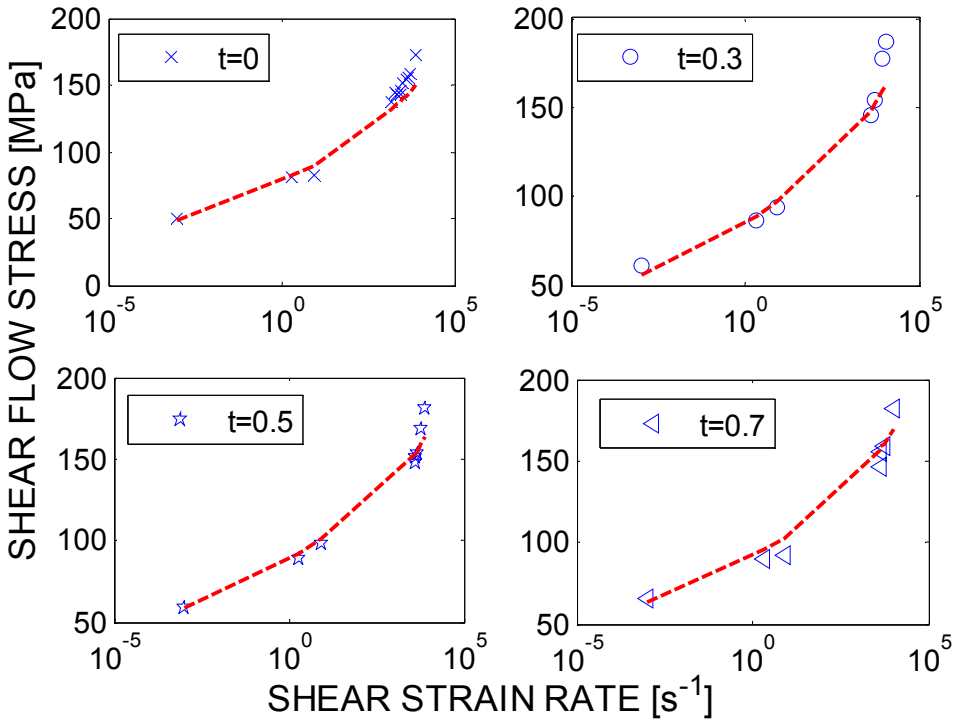

Figure 11: Shear flow stress vs. strain rate, for the different sleeve thicknesses. The dashed lines are obtained from eqn. (2).

Adiabatic shear failure of PMMA

This study shows that as confinement is applied, the measured stress is shifted upwards, as expected. The immediate post-peak strain-softening phase is followed in all cases by a steep slope leading to final failure. It is also observed that at the higher confinement levels, the previously negative tangent modulus of the strain-softening phase tends to become 0. This reduction in strain-softening indicates a more stable type of deformation, most likely due to the beneficial effect of the pressure over damage development. Damage itself consists of radial cracks at the lower strain rates, and of short cracks and voids in the adiabatic shear band at the higher rates. The final phase of the failure process is apparently not affected by the level of confinement. Yet, this "beneficial" effect of the confinement does not last, as the pressure and the strain rate increase. Suddenly, the "brittle" fragmentation failure mode becomes that of a "ductile" localized adiabatic shear band. This failure mode transition, from brittle cracking to ductile adiabatic shear is confirmed by scanning electron fractographic analysis without any ambiguity. Despite the different experimental conditions, this failure mode transition to a ductile regime is analogous to that observed by Winter (1975), and by Satapathy and Bless (2000) for this material. It is also identical to that reported for another brittle material, namely

ceramic, by Chen and Ravichandran (1997), who applied a direct confinement like in the present experiments. The present results extend these observations to a brittle polymer, showing the complementary effects of strain rate and confining pressure in inducing the observed transition in failure mode.

On the brittle-ductile failure mode transition

In their subsequent work on AlN ceramic, Chen and Ravichandran (2000) plotted their results for the shear failure stress, as a function of the hydrostatic pressure, together with those of previous authors on the same material tested at very high rates and confining pressures (plate-impact). The general plot consists of an initial linear relationship between the stress and the pressure, followed by a short transition, ended by a constant stress over a large range of pressures. These domains are the pressure sensitive (brittle) and pressure-insensitive (ductile-plastic) regimes respectively. Chartagnac (1981) provides analogous results for shocked PMMA, plotting the deviatoric stress as a function of the pressure. His data shows that the linear domain ends at S_{11}=210MPa and p=500MPa. We will adopt here Chen and Ravichandran's (2000) framework.

Table 3 contains the data of those points which displayed adiabatic shear failure, as shown in Figure 6.

Strain_rate [1/s]	**t** [mm]	**Calculated *q*** [MPa]	**Peak stress** [MPa]
4428	0.3	34.1	395
5500	0.3	34.1	408
3221	0.5	53.8	395
4111	0.5	53.8	416
2060	0.7	71.4	391
2257	0.7	71.4	401
2666	0.7	71.4	410
4873	0.7	71.4	463

Table 3: Parameters of the specimens that underwent adiabatic shear failure, from Fig. (6).

These parameters are now inserted into eqn. (2) where the hydrostatic pressure is given by $p = \frac{(\sigma_{flow} + 2q)}{3}$. The calculated shear stress and corresponding pressure are listed in Table 4.

Strain rate $\dot{\varepsilon}$ [1/s]	**Calculated** ***q*** [MPa]	**Peak stress** σ [MPa]	**Calculated** τ [MPa]	**Hydrostatic p** [MPa]
4428	34.1	395	160	154
5500	34.1	408	163	159
3221	53.8	395	160	168
4111	53.8	416	164	175
2060	71.4	391	159	178
2257	71.4	401	160	181
2666	71.4	410	162	184
4873	71.4	463	171	202

Table 4: Calculated shear stress from eqn.(2). $p = \frac{(\sigma_{flow} + 2q)}{3}$.

The results of this exercise show that the points that failed by adiabatic shear banding are all characterized by a relatively constant shear stress, $\bar{\tau} = 162\,\text{MPa}$, over a range of pressures $154 \le p \le 202\text{MPa}$. These results are plotted in Figure 12, along with calculated stresses over the complementary range of pressures using eqn. (2), for 3 characteristic (yet arbitrary) shear strain rates, namely $\dot{\gamma} = 100, 5000, 15000\,\text{s}^{-1}$. This graph illustrates the brittle and the ductile domains, including the strain rate effect that was not considered in previous works. This representation also rationalizes the brittle-ductile transition observed in PMMA in the general framework previously utilized for ceramic materials. The conclusion of that section is that this unified treatment of pressure induced brittle-ductile transition encompasses a wide range of materials systems, opening the way for further systematic investigations of other materials.

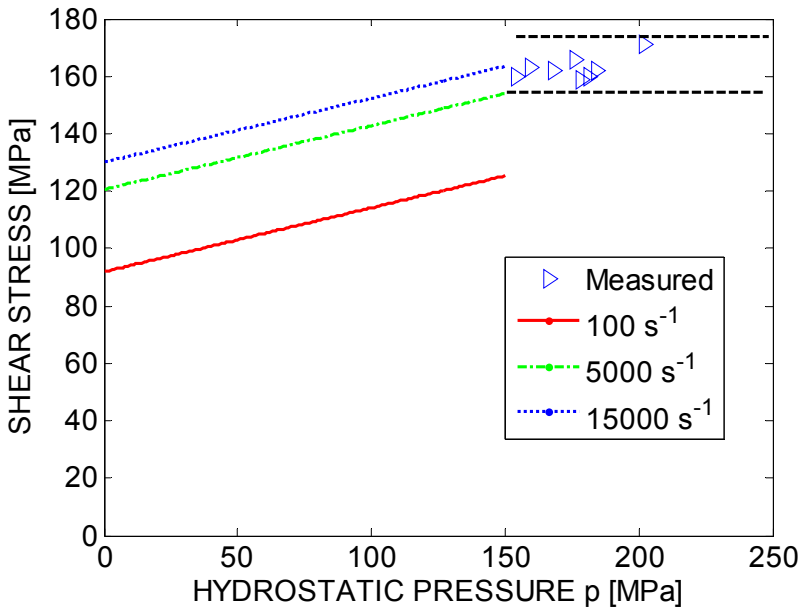

Figure 12: Shear stress vs. hydrostatic pressure. The points that failed by adiabatic shear are characterized by a constant (pressure independent) stress level over a large range of pressures. Below p=152 MPa, the material fails in a brittle (pressure dependent) mode at various strain rates. This figure illustrates the fact that lower strain rates require higher confining pressures.

SUMMARY and CONCLUSIONS

The dynamic flow and failure of confined commercial PMMA has been studied, and the main conclusions of this study are as follows:

1. PMMA exhibits brittle failure in the dynamic (high strain rate) regime only.
2. Applying confinement stabilizes the post peak flow curve by reducing the initial strain softening slope that precedes the final failure stage. This effect increases with the confining pressure.
3. A brittle to ductile failure mode transition appears in this material, as confining pressure is increased, for a fixed strain-rate.
4. The brittle failure consists of radial cracking and fragmentation. Ductile failure corresponds to the formation of a truncated conical plug whose envelope consists of elongated dimples and signs of thermal softening.
5. Scanning electron fractography reveals that the envelope of the conical plug is due to adiabatic shear banding.

6. Confining pressure and strain rate have opposite effects on the brittle-ductile transition. Namely, at low strain rates, a high confining pressure is required and vice-versa.
7. The rate and pressure dependence of the mechanical behavior of PMMA can be expressed by: $\tau_{flow} = 66.78\dot{\gamma}^{0.06933} + 0.223p$, for $10^{-3} \le \dot{\gamma} \le 10^{4}\ s^{-1}$.
8. The observed brittle-ductile transition is identical in its principle to that observed in other brittle (ceramic) material systems, for which the linear pressure-dependent behavior is followed by a constant, Mises-like, pressure independent flow.

Acknowledgement

The partial support of MAFAT-MOD (Grant #2006865) and the Israel Science Foundation (Grant #2007775) are gratefully acknowledged. So are the useful discussions with Dr. Y. Yeshurun.

APPENDIX

1. Stress analysis of the specimen

As mentioned in the introduction, the confined specimen experiences a confinement *q* that must be calculated separately, as shown in the next section. The determined confinement *q* can be subtracted to determine the pressure sensitive stress, σ(q), from which the Drucker-Prager parameters can be determined. For the confined specimens, the hydrostatic component is given by:

$$p = \frac{1}{3}\left(\sigma_{11}^{meas} + 2q\right) \quad \text{(A1)}$$

Where σ_{11}^{meas} is the measured longitudinal stress. The deviatoric longitudinal stress component is given by:

$$S_{11} = \frac{2}{3}\left(\sigma_{11}^{meas} - q\right) \quad \text{(A2)}$$

2. Determination of the confining pressure q

Consider a cylindrical sleeve with a, b, t being the internal radius, external radius and wall thickness respectively. The sleeve has a measured static yield strength $\sigma_S^s = 280\,\text{MPa}$ and dynamic yield strength $\sigma_S^d = 375\,\text{MPa}$ (the subscript *S* refers to sleeve, *s* and *d* meaning static and dynamic respectively).

The encased cylindrical specimen has a 6mm diameter, exactly matching the inner diameter of the sleeve, manufactured with 3 different thicknesses, namely t=0.3, 0.5 and 0.7 mm.

The plastic response of an internally pressurized cylindrical sleeve is a gradual process in which plasticity progresses from the inner toward the outer wall (Kachanov, 1974). The confining pressure, *q*, is given by the following expression, where ρ indicates the radius of the plastic-elastic zone:

$$q = \sigma_S\left[\ln\frac{\rho}{a} + \frac{1}{2}\left(1 - \frac{\rho^2}{b^2}\right)\right] \quad \text{(A3)}$$

The confining pressure can therefore be estimated from eqn. (A3), defining a lower and an upper bound at *a* and *b*, respectively, as shown in Table A1.

Thickness [mm]	$\frac{q}{\sigma_s}$	**q static [MPa]**	**q dynamic [MPa]**	$\bar{q}$ static **[MPa]**	$\bar{q}$ dynamic **[MPa]**
0.3	0.087-0.095	24.3-26.7	32.5-35.7	**25.5**	**34.1**
0.5	0.133-0.154	37.1-43.2	49.7-57.8	**40.1**	**53.8**
0.7	0.171-0.210	48.0-58.7	64.2-78.6	**53.3**	**71.4**

Table A1: Confining parameters of the various sleeves used in this work. The average values of the 2 rightmost columns are employed throughout this work. The lower value corresponds to yielding at r=a, and the higher one for r=b.

Table A1 shows that the ratio of the upper to lower bound values of q is of the order of 1.2 for both static and dynamic configurations. This ratio is relatively modest, so that the average value of the confining pressure is subsequently used as a representative value throughout this work.

The hoop strain is usually monitored by means of a strain gauge (Bardia and Narasimhan, 2006; Lu and Ravichandran, 2003; Ma and Ravi-Chandar, 2000). However, the present work did not include this item since the primary goal of the experiment was to record the stress-strain curve of the specimen for a given calculated confinement, rather that each individual components of the stress tensor. Consequently, one needs to ascertain that the sleeve is actually plastic during the experiment, such as to provide a constant level of confinement. Preliminary finite element simulations were conducted to assess the longitudinal strain of the specimen at which yielding of the sleeve is completed. A two-dimensional axisymmetric model of the confined specimen was run on the commercial FE package Autodyn (AUTODYN, 2006). The PMMA and the aluminum alloy sleeve were modeled according to Von Mises and Steinberg strength model available in Autodyn library. Figure A1 shows the model and geometrical dimensions.

The results of the finite element simulation confirm the assumption that the sleeve completes its yielding process at an early stage of the loading process where the specimen is still elastic $(\varepsilon = 0.03)$, as shown in Figure A2.

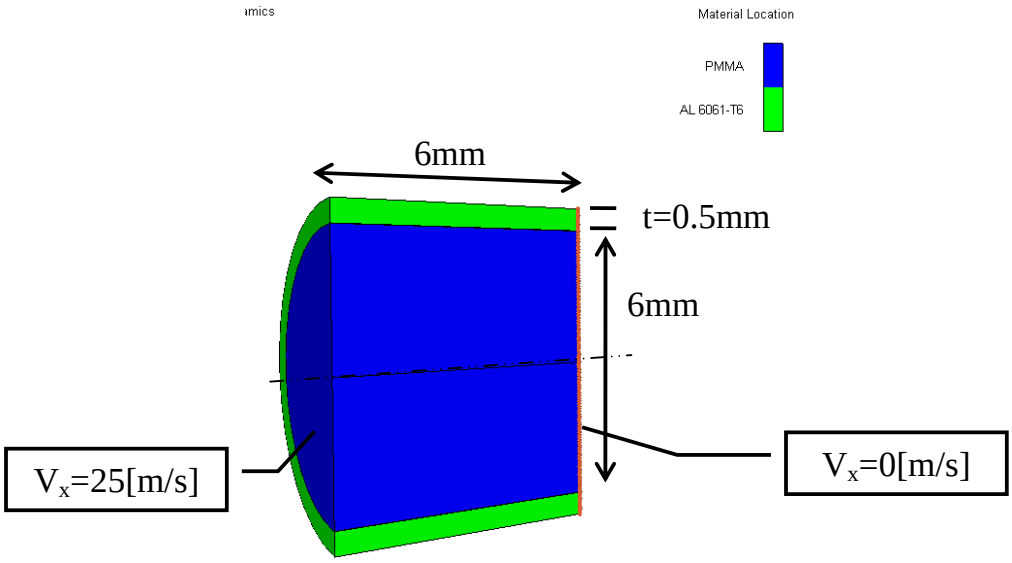

Figure A1: Finite element model of the encased specimen.

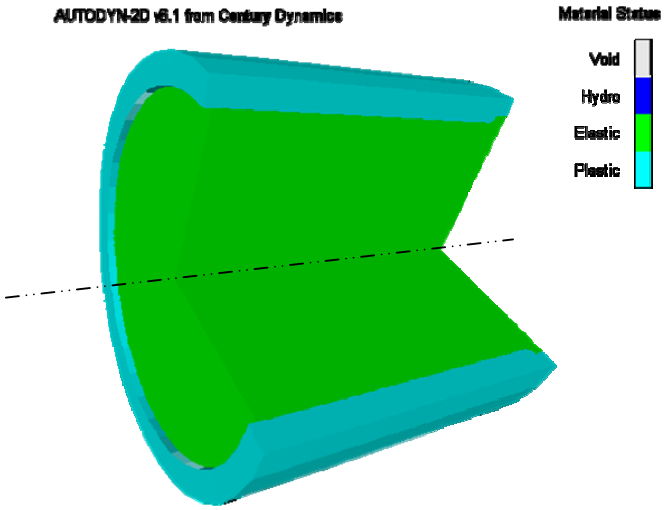

Figure A2: Result of the finite element simulation showing that the PMMA specimen is still elastic $(\varepsilon = 0.03)$ while the sleeve is completely yielded.

REFERENCES

Arruda, E.M., Boyce, M.C., Jayachandran, A., 1995. Effects of strain rate, temperature and thermomechanical coupling on the finite strain deformation of glassy polymers. Mechanics of Materials 19, 193-212.

AUTODYN, 2006. Theory Manual (6.1). Century Dynamics Inc.

Bardia, P., Narasimhan, R., 2006. Characterisation of pressure-sensitive yielding in polymers. Strain 42, 187-196.

Blumental, W.R., Cady, C.M., Lopez, M.F., III, G.T.G., Idar, D.J., 2001. Influence of temperature and strain rate on the compressive behavior of PMMA and polycarbonate polymers. Los Alamos Report.

Bridgman, P.W., 1945. Flow and Fracture. AIME Trans. 162, 569-583.

Chartagnac, P.F., 1981. Determination of mean and deviatoric stresses in shock loaded solids. J. Appl. Phys. 53 (2), 948.953-

Chen, W., Ravichandran, G., 1996. Static and dynamic compressive behavior of aluminum nitride under moderate confinement. J. Am. Ceram. Soc. 79 (3), 579-584.

Chen, W., Ravichandran, G., 1997. Dynamic compressive failure of glass ceramic under lateral confinement. J. Mech. Phys. Solids 45 (8), 1303-1328.

Chen, W., Ravichandran, G., 2000. Failure mode transition in ceramics under dynamic multiaxial compression Int. J. Fract. 101 (1-2), 141-159.

Christensen, R.M., 1982. Theory of Viscoelasticity: An Introduction. Academic Press, New York.

Constable, I., Williams, J.G., Burns, D.J., 1970. Fatigue and thermal softening of thermoplastics. J. Mech. Engng. Sci. 12 (1), 20-29.

Hanina, E., Rittel, D., Rosenberg, Z., 2007. Pressure sensitivity of adiabatic shear banding in metals. Applied Physics Letters 90 (2), 021915.

Kachanov, L.M., 1974. Foundations of the Theory of Plasticity. Mir, Moscow.

Knauss, W.G., Ravi-Chandar, K., 1985. Some basic problems in stress wave dominated fracture. Int. J. Fract. 27 (3-4.127-143 ,(

Kolsky, H., 1949. An investigation of the mechanical properties of materials at very high rates of loading. Proc. Phys. Soc. London 62-B, 676-700.

Li, Z.H., Lambros, J., 2001. Strain rate effects on the thermomechanical behavior of polymers Int .J. Solids & Structures 38 (20), 3549-3562.

Lu, J., Ravichandran, G., 2003. Pressure-dependent flow behavior of Zr41.2Ti13.8Cu12.5Ni10Be22.5 bulk metallic glass J. Mat. Res. 18 (9), 2039-2049.

Ma, Z., Ravi-Chandar, K., 2000. Confined compression: A stable homogeneous deformation for constitutive characterization. Exp. Mech. 40 (1), 38-45.

Moy, P., Weerasooriya, T., Chen, W., Hsieh, A., 2003. Dynamic stress-strain response and failure behavior of PMMA. ASME International Mechanical Engineering Congress. ASME APPLIED MECHANICS DIVISION -PUBLICATIONS- AMD, pp. 105-110.

Quinson, R., Perez, J., Rink, M., Pavan, A., 1997. Yield criteria for amorphous glassy polymers J. Matls. Sc. 32 (5), 1371-1379.

Ramsey, J.M., Chester, F.M., 2004. Hybrid fracture and the transition from extension fracture to shear fracture Nature 428 (6978), 63-66.

Renshaw, C.E., Schulson, E.M., 2001. Universal behaviour in compressive failure of brittle materials Nature 412 (6850), 897-900.

Rittel, D., 1999. The conversion of plastic work to heat during high strain rate deformation of glassy polymers. Mechanics of Materials 31 (2), 131-139.

Rittel, D., 2000a. Experimental investigation of transient thermoplastic effects in dynamic fracture. International Journal of Solids and Structures 37.2901-2913 ,(21)

Rittel, D., 2000b. An investigation of the heat generated during cyclic loading of two glassy polymers. Part I: experimental. Mechanics of Materials 32 (3), 131-147.

Rittel, D., 2000c. A note of the dynamic failure of PMMA. Int. J. of Fracture 106 (2), L3-L8.

Rittel, D., Hanina, E., Ravichandran, G., 2007. A note on the direct determination of the confining pressure of cylindrical specimens. Exp. Mech. in press.

Rittel, D., Maigre, H., 1996. An investigation of dynamic crack initiation in PMMA. Mechanics of Materials 23 (3), 229-239.

Rosenberg, Z., Surujon, Z., Yeshurun, Y., Ashuach, Y., Dekel, E., 2005. Ricochet of 0.3 " AP projectile from inclined polymeric plates Int. J. Impact Engng. 31 (3), 221-233.

Satapathy, S., Bless, S., 2000. Deep punching PMMA Exp. Mech 40 (1), 31-37.

Tresca, H., 1879. Sur la fluidité et l'écoulement des corps solides. Annales du Conservatoire des Arts et Métiers 4.

Trojanowski, A., Ruiz, C., Harding, J., 1997. Thermomechanical properties of polymers at high rates of strain. J. Physique Coll. C 3, 447-452.

Van-Melick, H.G.H., Govaert, L.E., Van-Casteren, I.A., Li, H., Jansen, B.J.P., Meijer, H.E.H., 1997. Deformation and fracture of polymer systems. Eindhoven University of Technology.

Ward, I.M., 1983. Mechanical Properties of Solid Polymers. J. Wiley and Sons, New York, NY.

Winter, R.E., 1975. Adiabatic shear of titanium and polymethylmethacrylate. Phil. Mag. 31 (4), 765-773.